Research Article | Vol. 0, No. 0 / 00 00 0000 / Optics Express 1

Optics EXPRESS

High-power, high-efficiency, all-fiberized-laser-pumped, 260-nm, deep-UV laser for bacterial deactivation

QIANG FU,[1] NIALL HANRAHAN,[2] LIN XU,[1,*] SIMON LANE,[2] DI LIN,[1] YONGMIN JUNG,[1] SUMEET MAHAJAN,[2] AND DAVID J. RICHARDSON[1]

[1] *Optoelectronics Research Centre, University of Southampton, Southampton, SO17 1BJ, UK*
[2] *Institute for Life Sciences and School of Chemistry, University of Southampton, Southampton, SO17 1BJ, UK*
[*] *l.xu@soton.ac.uk*

Abstract: We report a 5.8-W deep-ultraviolet (DUV) laser obtained from frequency-quadrupling of an all-fiberized ytterbium-doped fiber (YDF) master oscillator power amplifier (MOPA). The MOPA system delivers 585 ps pulses at 1040 nm with a maximum available output power of 23.5 W for nonlinear frequency conversion. A lithium triborate (LBO) crystal and a beta barium borate (BBO) crystal are employed for second- and fourth-harmonic generation (FHG), respectively. At a repetition rate of 1.6 MHz, a maximum DUV output power of 5.8 W is obtained at 260 nm with a corresponding pulse energy of 3.6 μJ and maximum peak power of at least 6.9 kW. A 1μm-to-260nm conversion efficiency of 26.4% is achieved at a DUV output power of 5.8 W. To the best of our knowledge these results represent the highest-average-power fiberized-laser-pumped DUV laser, as well as the most efficient DUV generation based on BBO crystals to date. We further demonstrate application of the pulsed DUV laser in bacterial disinfection achieving an inactivation efficiency of 99.999% for E-coli bacteria at a DUV exposure of 7 mJ/cm^2.

1. Introduction

High-power pulsed DUV lasers with high photon energy have various applications in photolithography [1], material processing [2], spectroscopy [3], and biomedicine [4]. Harmonic frequency conversion has become an important approach in the realization of DUV lasers exploiting nonlinear crystals pumped by advanced 1-μm laser sources, including titanium-sapphire lasers and neodymium-doped (Nd-doped) or ytterbium-doped bulk or fiber lasers. YDF lasers have attracted great attention in particular owing to their compact nature, high output power, high efficiency and reliability, good beam quality, and suitability for simple air-cooling. Meanwhile, good-quality nonlinear crystals are vitally important for harmonic DUV generation and only a few suitable and commercially available crystals have been developed over the years, such as BBO, caesium lithium borate (CLBO), and potassium beryllium fluoroborate. BBO and CLBO are the most commonly used crystals for high-power DUV laser development due to their high nonlinear coefficients, high laser damage thresholds and mature growth techniques. Compared with CLBO, BBO with a lesser hygroscopic susceptibility and larger nonlinear coefficients is the more favorable choice for high-power, long term DUV operation.

Optical fiber based laser systems have been demonstrated to provide powerful pump sources for high-power DUV systems, including free-space coherently-combined YDF amplifiers [5] and YDF-laser-seeded bulk amplifiers [6,7]. Compared with these fiber laser systems, which used free-space light coupling, an all-fiberized laser configuration offers advantages in terms of

#441248 https://doi.org/10.1364/OE.441248
Journal © 0000 Received 23 Aug 2021; revised 4 Oct 2021; accepted 4 Oct 2021; published 00 00 0000

Optics EXPRESS

reduced alignment sensitivity, better reliability, and a smaller physical footprint. However, in order to achieve high-power and high-efficiency frequency conversion to the DUV, the pump lasers need to offer output pulses with high peak power, narrow spectral linewidth and good beam quality. These requirements bring challenges for all-fiberized lasers due to deleterious nonlinear effects, such as self-phase modulation (SPM) and stimulated Brillouin scattering (SBS). There have only been a few reports on fiberized-laser-pumped DUV lasers over the years. In 2015, S. C. Kumar et al. demonstrated a commercial-fiber-laser-pumped ~17-ps-pulsed DUV (266nm) laser with an output power of 1.8 W based on a 10-mm-long BBO crystal [8]. By cascading another 10-mm-long BBO crystal in a spatial walk-off compensation scheme, thereby sacrificing compactness and alignment insensitivity, the DUV output power was increased to 2.9 W but at an overall conversion efficiency that was still relatively low at 17.2% (1μm-to-266 nm) [9]. In parallel work from our research group, Jing et al. demonstrated a YDF-MOPA-pumped DUV laser at 274 nm with 2 W output power and 16.9% conversion efficiency (1μm-to-274 nm) [10]. However, in order to optimize the MOPA, which operated at a wavelength of 1097 nm (much longer than the YDF gain peak wavelength), a long length of YDF and a free-space coupled backward-pump scheme was employed in the final amplifier. This resulted in relatively low efficiency amplification (53% slope efficiency) and restricted power scaling.

In this paper we develop a YDF MOPA system operating at 1040 nm in a fully-fiberized format with 80% slope efficiency and demonstrate DUV frequency conversion to 260-nm, providing 5.8-W average power and a 26.4% 1μm-to-260nm conversion efficiency. The YDF MOPA delivers 585-ps pulses at a repetition rate of 1.6 MHz with an average output power of 23.5 W available for frequency conversion. We use an LBO crystal for second-harmonic generation (SHG) achieving a maximum average power of 16.2 W at 520 nm with a conversion efficiency (1μm-to-520nm) of ~69%. A 5-mm-long BBO crystal is then employed for FHG generating a DUV output power of 5.8 W at 260 nm with a corresponding pulse energy / peak power of 3.6 μJ / 6.9 kW. We report conversion efficiencies of 38.4% from 520 nm to 260 nm and ~26.4% from 1 μm to 260 nm, respectively. To the best of our knowledge, these results represent the highest-average-power fiber-laser-pumped DUV laser (two-times higher than the state-of-the-art [9]) as well as the most efficient DUV generation based on BBO crystals to date. In addition, we show application of the DUV laser to bacterial (E. Coli) disinfection achieving high (99.999%) and efficient bacterial inactivation (7 mJ/cm^2 total DUV dose). The system is shown to offer more efficient disinfection than a continuous wave incoherent DUV LED source.

2. All-fiberized high-power YDF MOPA development

2.1. Experimental setup of the YDF MOPA

Figure 1 illustrates the experimental setup of the polarization-maintaining YDF MOPA system, which consisted of four pre-amplifier stages and a final power amplifier. The seed laser was a continuous-wave (CW) narrow-linewidth (<300 kHz) laser diode (Toptica photonics, DL pro), set to a wavelength of 1040-nm and with a fiber-pigtailed output delivering ~10 mW of average power. The CW signal was initially amplified to 80 mW by a core-pumped YDF amplifier (1st Pre-Amp, Fig. 1), consisting of a 0.85-m-long polarization-maintaining YDF (Nufern, PM-YDF-5/130) that was forward pumped by a 975-nm single-mode laser diode through a wavelength-division multiplexer. A fiber-pigtailed electro-optic modulator (EOM, extinction ratio >30 dB, NIR-MX-LN-10, Photline) was employed to modulate the CW signal and to generate 585-ps pulses at a repetition rate of 8 MHz with an output power of ~100 μW. The pulsed signal was then amplified to ~50 mW by two YDF amplifiers (2nd Pre-Amp and 3rd Pre-Amp, Fig. 1), whose experimental configurations were the same as the 1st Pre-Amp. A fiber-pigtailed acoustic-optic modulator (AOM, extinction ratio >45 dB, MT110-IR20-Fio-PM, AA Opto Electronic) was employed to reduce the repetition rate of the pulsed signal to 1.6 MHz and also to suppress the inter-pulse amplified spontaneous emission, which resulted in a reduced signal power of 5 mW with which

Optics EXPRESS

to seed the 4th Pre-Amp (Fig. 1). The EOM and AOM were synchronously driven by an arbitrary waveform generator (AWG, 7122C, Tektronix). In the 4th Pre-Amp, the signal power was boosted to 120 mW using a 3-m-long 10-µm-core YDF (Nufern, PLMA-YDF-10/125-VIII) that was forward-cladding-pumped by a multimode laser diode (975 nm). The final power amplifier (Fig. 1) was forward-cladding-pumped with a 2.1-m-long 25-µm-core large-mode-area YDF (PLMA-YDF-25/250), and the output facet of the YDF was spliced with an 8° angle-cleaved glass endcap to prevent detrimental back reflection. A fiber-pigtailed 1% tap coupler was placed before the final amplifier to provide monitoring of any backward SBS. The seed laser and all pre-amplifiers were followed by fiber-pigtailed isolators to prevent back-reflected light.

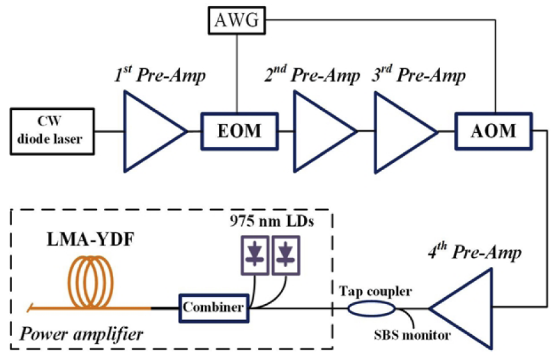

Fig. 1. Schematic of the YDF MOPA system. CW diode laser: continuous-wave diode laser; Pre-amp: pre-amplifier; AWG: arbitrary waveform generator; EOM: electro-optic modulator; AOM: acousto-optic modulator; SBS monitor: stimulated Brillouin scattering monitor; LDs: laser diodes; LMA-YDF: large-mode-area ytterbium-doped fiber.

2.2. YDF MOPA experimental results and discussion

In the picosecond and nanosecond pulse regimes, efficient nonlinear frequency conversion to visible or DUV wavelengths requires the pump source to have a high peak power as well as a narrow spectral linewidth that fits within the pump acceptance bandwidths of the nonlinear crystals. Pulse carving from a narrow-linewidth CW laser and amplifying the resulting pulsed signal in a fiber MOPA is an effective solution to this requirement. However, amplification of narrow-linewidth signals in YDFs can also lead to SBS generation, which can limit power scaling [11,12]. In our YDF MOPA design, the SBS effect only became observable in the final power amplifier. In order to investigate and mitigate SBS effects in this amplifier the MOPA system performance was characterized at different pulse durations (2 ns, 1 ns, 585 ps) by adjusting the drive signals to the EOM and the AOM with the AWG. Figure 2 (a) shows the monitored SBS spectra for different pulse durations and peak powers from the power amplifier. For 1-ns and 2-ns pulsed operation, an SBS spectral peak increase was clearly observed at peak powers of 28 kW and 14 kW, respectively. In contrast, for 585-ps pulsed operation, the SBS spectral peak only increased to the same power level at a peak power of 56 kW. This is as expected as use of shorter pulse durations (with correspondingly wider spectral bandwidths) should increase the SBS threshold [13]. The slight spectral broadening of the central peak, as well as the formation of spectral side lobes (below 20-dB from the peak in Fig. 2 (b)), were due to the effects of SPM. At a peak power of 56 kW the majority of the optical power (calculated to be 85%) was contained within the central peak, with a bandwidth of 0.17 nm (spectra between the two dashed lines in Fig. 2 (b)). This spectral characteristic is sufficient to allow the source to be employed as a fundamental pump source for frequency quadrupling in a commercially available 5-mm-long BBO crystal with a pump acceptance bandwidth of ~0.2 nm. The inset of Fig. 2 (b) shows the

Optics EXPRESS

output spectra of the YDF MOPA over a wide spectral window indicating the absence of any other nonlinear effects, such as stimulated Raman scattering. DUV frequency conversion was investigated and characterized at the same average output power at repetition rates of 1.6 MHz and 800 kHz.

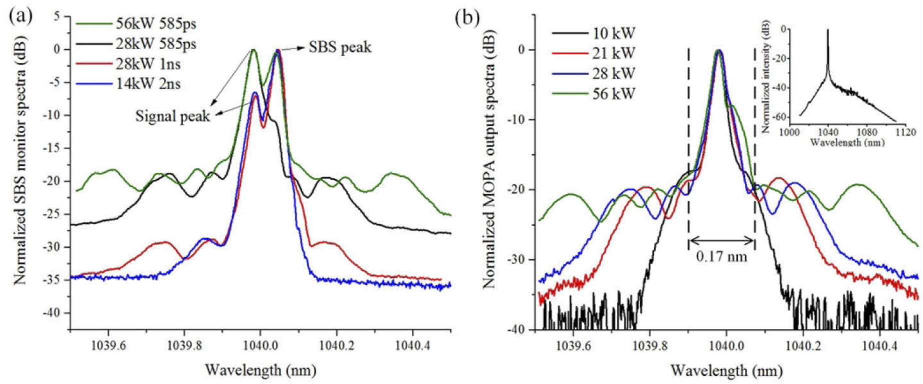

Fig. 2. (a) Normalized spectra from the SBS monitor port at 585 ps, 1 ns, and 2 ns 1040-nm pulse duration and with different peak powers (0.01-nm resolution). (b) Output spectra of the YDF MOPA at a pulse duration of 585 ps and different output peak powers (0.01-nm resolution). Inset: Output spectra of the YDF MOPA over a large wavelength scale (1-nm resolution).

Figure 3 shows the output power characteristics of the final stage of the YDF MOPA system. At a slope efficiency of 80%, a maximum output power of 26.6 W was obtained for 35.6 W of injected pump power, corresponding to a power conversion efficiency of 75% (975nm-to-1040nm). The inset of Fig. 3 shows the temporal profile of a 1040-nm pulse with a full-width-at-half-maximum (FWHM) of 585 ps, which was characterized using an InGaAs photodetector (Thorlabs, DET-08CFC, 5 GHz bandwidth). With a repetition rate of 1.6 MHz (800 kHz), the maximum pulse energy and peak power were calculated to be 17 μJ (34 μJ) and 28 kW (56 kW), respectively. The polarization extinction ratio of the output beam was measured to be >20 dB, and its beam quality was characterized to be M^2<1.1.

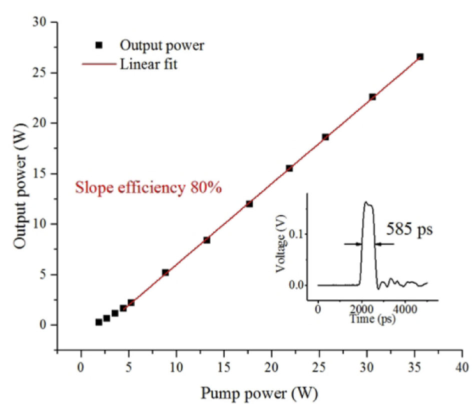

Fig. 3. Output power characteristics of the YDF MOPA system. Inset: temporal profile of the 1040 nm pulses at a pulse duration of 585 ps.

3. Nonlinear frequency conversion to the DUV

3.1. Experimental setup for second- and fourth- harmonic generation

A simple single-pass configuration was used for nonlinear frequency conversion to the DUV, as shown in Fig. 4. In order to avoid back-reflection of light into the YDF MOPA, the collimated beam of the YDF MOPA output was propagated through a polarization sensitive isolator together with two half-wave plates (HWP1, HWP2, Fig. 4). HWP1 adjusted the polarization direction to achieve maximum output after the isolator, whilst HWP2 was used to achieve optimal phase matching for SHG. The 1040-nm laser beam was then focused into an LBO crystal with a beam waist of 75 μm. The available average power of the 1040-nm laser was 23.5 W (measured immediately before the LBO) due to the non-negligible losses of the isolator, lens, half-wave plates and other directing mirrors (not shown in Fig. 4). The LBO was designed for type-I non-critical phase matching for SHG with dimensions of 4×4×25 mm (Eksma optics) and cut angles of θ=90°, φ=0°. We chose LBO for high-power SHG due to its high damage threshold, relatively high nonlinear coefficient, non-critical phase matching capability, and no spatial walk-off. The LBO was antireflection (AR) coated at 1040 nm and 520 nm, and it was mounted in an oven with a set temperature of 175.6°C to allow maximum nonlinear conversion efficiency. Two dichroic mirrors (DM1 and DM2, Thorlabs, HBSY12) were used to filter out the residual 1040 nm beam. The 520 nm beam was collimated and focused into a BBO crystal, which was 4×4×5 mm (Castech) with cut angles of θ=49.3°, φ=0° for type-I critical phase matching at room temperature. The BBO was AR coated for 520 nm and 260 nm, which also prevented hygroscopic deterioration. The crystal was mounted on a 5-axis transitional stage to allow precise control of the crystal angle and position. Two dichroic mirrors (DM3 and DM4, Thorlabs, HBSY134) were employed to couple out the generated DUV beam at 260 nm.

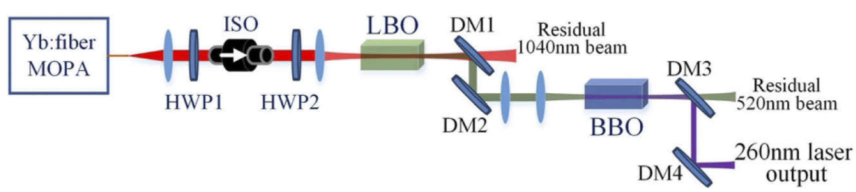

Fig. 4. Schematic of the DUV frequency conversion. HWP: half-wave plate; ISO: isolator; DM: dichroic mirror.

3.2. Experimental results and discussion for DUV frequency conversion

Figure 5 depicts the measured SHG output power with respect to the 1040-nm pump power, at the same pump beam waist of 75 μm and at different repetition rates of 800 kHz (Fig. 5 (a)) and 1.6 MHz (Fig. 5 (b)). At 800 kHz, an output power of 10.8 W was obtained at a pump power of 15.5 W, with a maximum conversion efficiency of 69.7%. However, when the pump power was more than 15.5 W, the SHG power and conversion efficiency started to roll-off due to back-conversion. In contrast, at a repetition rate of 1.6 MHz (Fig. 5 (b)), up to 16.2 W of 520-nm laser power was generated at the maximum pump power of 23.5 W, with a conversion efficiency of 68.9%. The SHG conversion efficiency gradually increased with increasing pump power, and no obvious roll-off was observed due to the reduced pump intensities in this case. The temporal profiles of the SHG pulses were characterized using a Si detector (Thorlabs, DET025A, 2-GHz bandwidth) and a digital communication analyzer (Agilent, Infiniium 86100C, 20 GHz bandwidth). Figure 6 (a) shows the measured temporal profile with a FWHM of 527 ps, which was slightly shorter than that of the 1040 nm pump (Fig. 3 inset). The small change in the temporal profile was likely due to the nonlinear pulse narrowing effect [6,14]. Figure 6 (b) shows the beam quality measurement result for the SHG beam at maximum output power, with an M^2 factor of 1.05 and 1.03 for the horizontal (x) and vertical (y) directions, respectively. The inset of Fig. 6 (b) shows the measured SHG spectra with a 0.05-nm resolution.

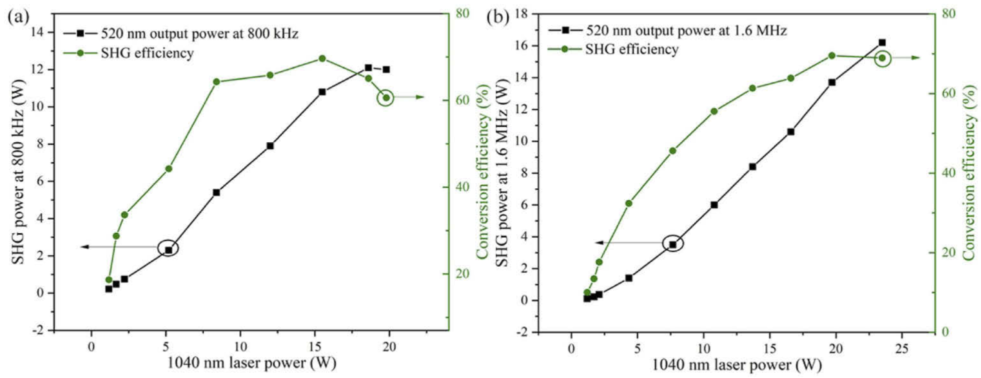

Fig. 5. Output power and conversion efficiency of SHG at a repetition rate of (a) 800 kHz and (b) 1.6 MHz.

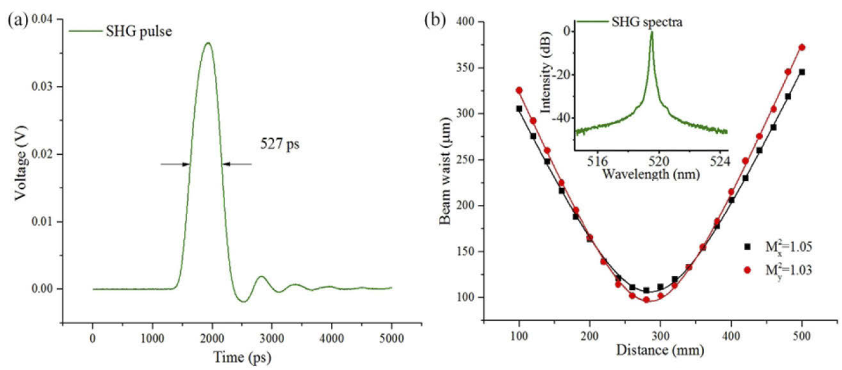

Fig. 6. (a) Temporal profile for the SHG pulse. (b) Beam quality measurements for the SHG beam. Inset: SHG spectra measured at a resolution of 0.05 nm.

For the FHG, we first operated the YDF MOPA at a repetition rate of 800 kHz for high peak power DUV output. With a pump beam waist of 30 μm inside the BBO crystal, a maximum DUV output power of 3.1 W was achieved at a pump power of 10 W (blue circles in Fig. 7 (a)). Although the 30μm-beam-waist was much bigger than that for the confocal focusing condition (~16 μm), the DUV output power saturated when the pump power was higher than ~8 W (peak intensity ~1.3 GW/cm^2). No damages of crystal coatings were observed during the experiment, although that power was close to the quoted damage threshold (1.5 GW/cm^2) of the coatings on the crystal facets. Potential causes of the power saturation are high-intensity-induced two-photon absorption (TPA) and associated thermal effects [9,15,16]. In order to mitigate these effects, we halved the pump power intensities by either doubling the YDF MOPA repetition rate (from 800 kHz to 1.6 MHz) or enlarging the pump beam waist (from 30 μm to 42 μm), as shown by the squares and triangles in Fig. 7 (a), respectively. We can see that at a pump power of 10 W, better DUV output performance was achieved for the 1.6-MHz-repetition-rate and 30-μm-beam-waist case with a maximum output power of 3.6 W, while only 2.5 W output power was obtained for the larger 42 μm pump beam waist at a repetition rate of 800 kHz. Although the same pump intensity is used in these two cases, tighter focusing can lead to a smaller overlap between the SHG and FHG beams due to spatial walk-off (walk-off angle of 85 mrad), which in turn benefits TPA mitigation [17]. By further increasing the pump power for the case of the pump beam waist of 30-µm and the repetition rate of 1.6 MHz (Fig. 7 (a) squares), a maximum output power of 5.8 W was obtained at a pump power of 15.1 W, as shown in Fig. 7 (b). Figure 7 (b) also plots the conversion efficiencies for both green-to-DUV (520 nm to 260 nm) and IR-to-DUV (1040 nm to 260 nm) showing a maximum IR-to-DUV (green-to-DUV) conversion efficiency of 26.4% (38.4%). In operation, the TPA effect was found to influence the phase matching when the DUV output power reached ~1.6 W. The calculated DUV power absorption at this power level is ~200 mW which on conversion into heat was estimated to increase the crystal temperature by 4°C. This temperature increase would be expected to result in an appreciable phase mismatch. This was in accord with our observation that the BBO crystal needed to be adjusted to slightly offset the phase match angle to optimize the output power at DUV output power above 1.6 W. The power stability of the DUV was measured at 5.8 W output power over 15 mins, as plotted in Fig. 8 (a). It can be seen that the output power showed a slow decrease to 5.4 W in 15 minutes, which was probably due to the thermal accumulation in the crystal and some mechanical drift of the mounting stage, however, the output power can be readily recovered by small adjustment of the crystal angle (Fig. 8 (a)). Over 6 W of DUV output power was observed at the maximum pump power of 16.2 W at 520 nm (not shown in Fig. 7 (b)), but the output power was quite unstable, possibly due to the more severe TPA. Moreover, crystal damage was observed at this high pump power during long-term operation. Due to the lack of available fast DUV photodetectors, the DUV pulse was not measured but it can be assumed to have a similar or shorter pulse duration compared to the SHG pulse due to nonlinear pulse narrowing [6,8,14]. Therefore, the maximum DUV peak power can be estimated to be at least 6.9 kW. The inset of Fig. 8 (a) shows the DUV spectra measured at a resolution of ~1 nm by a UV spectrometer (Ocean Insight, HR2000+CG Spectrometer). The beam quality of the DUV beam was characterized with a pyroelectric beam profiler (Nanoscan, Ophir) giving M_x^2=3.4 and M_y^2=1.7 at an output power of 5.8 W, as shown in Fig. 8 (b), and the elliptical beam shape is due to spatial walk-off in the BBO.

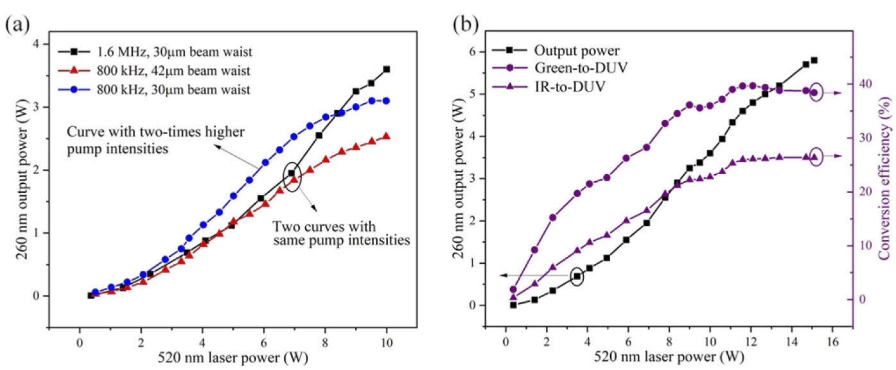

Fig. 7. (a) Output power characteristics for different 520 nm pump conditions. (b) Output power characteristics and conversion efficiencies of FHG at a repetition rate of 1.6 MHz and a beam waist of 30 µm.

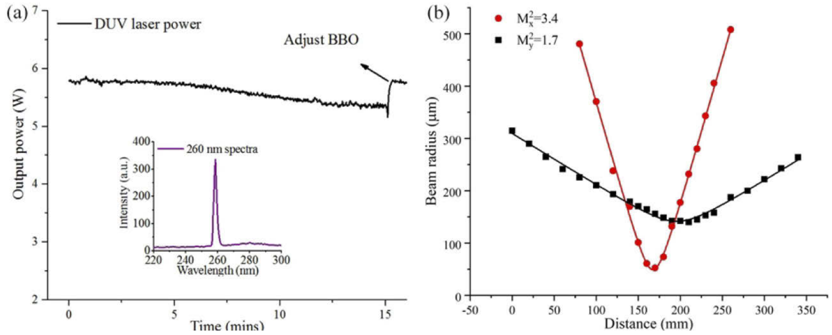

Fig. 8. (a) Power stability measurement of DUV laser at 5.8 W. Inset: DUV laser spectra with ~1 nm resolution. (b) DUV beam quality measurement at an output power of 5.8 W.

4. Application of DUV Laser to Bacterial Inactivation

Although DUV laser systems are useful in lithography and materials processing applications, we were motivated by the ongoing COVID-19 pandemic to test our DUV system for pathogen disinfection. Recently, interest in UV disinfection (inactivation and/or sterilisation) for bacteria, fungi and viruses has seen a resurgence [18,19].

There is particular interest in the UVC range (200-280 nm) due to the molecular absorption of biomolecules, especially DNA which maximally absorbs around 260 nm [20]. Here, an application of our DUV laser system for bacterial inactivation is briefly demonstrated, showing its effectiveness at preventing the growth of E. Coli in a ~150 μm thin liquid film of growth medium, which closely replicates the thickness of droplets from the respiratory system.

Figure 9 shows the survival assay of live E. Coli bacteria relative to experimental control. As expected, an increase in DUV dose results in a decrease in bacteria survival (as a proportion of the control). This trend is observed both for illumination using our DUV laser system and with a separate continuous wave DUV LED system used a reference (see Supplement 1). Survival of 1 in 10^5 of bacteria was measured following 260 nm DUV illumination with the laser at a dose of 7 mJ/cm^2 (Fig. 9). This corresponds to an inactivation efficiency of 99.999%, which compares favourably with that achieved using a DUV LED illumination source (See Supplement 1) and with

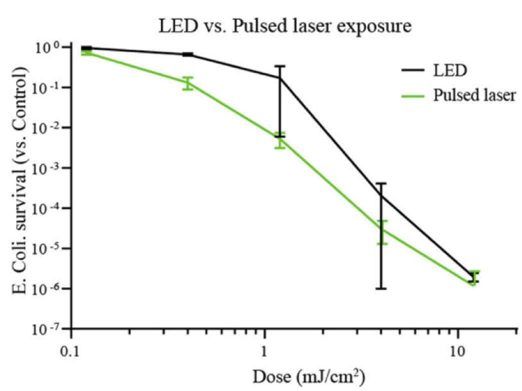

Fig. 9. Survival assay of live E. Coli bacteria relative to experimental control with changing DUV dose on exposure to the pulsed DUV laser system and an LED source. The y-axis shows the proportion of bacteria remaining in samples that were exposed to DUV doses compared to unexposed samples.

disinfection efficiencies presented in the literature, although comparisons must be made carefully given the differences in sample presentation [21,22]. Note that the units for DUV dose refer to average power, and not to pulse energy. The low 1-mW average power used in this experiment, less than 0.02% of the available maximum, highlights the potential to significantly scale up this system for particular applications, including (1) in continuous or flow-based sterilisation – where speed of sterilisation is of critical importance, (2) across large areas – where high power density can be maintained, or (3) where careful spatial/temporal control of the optical properties of the DUV illumination source are important, here the laser can outperform incoherent illumination sources such as LEDs and lamps.

5. Conclusion

In summary, we have demonstrated a high-efficiency, high-power, BBO-based 260-nm DUV sub-nanosecond pulsed laser source obtained by frequency quadrupling of an all-fiberized YDF MOPA system. The YDF MOPA was developed to simultaneously achieve high peak power and narrow spectral linewidth for efficient frequency conversion. For the DUV generation, a maximum 260-nm output power of 5.8 W was obtained at a repetition rate of 1.6 MHz, corresponding to a pulse energy of 3.6 µJ and a peak power of >6.9 kW. Conversion efficiencies of 26.4% and 38.4% were achieved for IR-to-DUV and green-to-DUV, respectively. These results represent the highest DUV output power from an all-fiberized fiber laser pumped FHG source to date. We further demonstrated the effectiveness of this laser system for bacterial inactivation, achieving fast inactivation of live E Coli bacteria presented as a liquid sample in a strongly absorbing medium.

Funding. Engineering and Physical Sciences Research Council (EP/P030181/1, EP/T020997/1). Q1

Acknowledgements. The authors acknowledge support from Dr Bill Brocklesby's group for loan of their spectrometer to measure the DUV spectra and fruitful discussions with Prof. David Shepherd. Equipment support from the Biomolecular Core Group of facilities (School of Biological Sciences) and funding from Engineering and Physical Sciences Research Council Impact Acceleration 2020/21 award are also gratefully acknowledged.

Disclosures. The authors declare no conflicts of interest.

Data availability. Data contained in this paper is openly available in Ref. [23].

Supplemental document. See Supplement 1 for supporting content.

References

1. C. Wagner and N. Harned, "Lithography gets extreme," Nat. Photonics **4**(1), 24–26 (2010).
2. P. Herman, R. Marjoribanks, A. Oettl, K. Chen, I. Konovalov, and S. Ness, "Laser shaping of photonic materials: deep-ultraviolet and ultrafast lasers," Appl. Surf. Sci. **154-155**, 577–586 (2000).
3. S. Banerjee, Z. Chen, and R. Fedosejevs, "High resolution scanning microanalysis on material surfaces using UV femtosecond laser induced breakdown spectroscopy," Optics and Lasers in Engineering **68**, 1–6 (2015).
4. D. L. Elliott, *Ultraviolet laser technology and applications*, Academic press (2014).
5. M. Müller, A. Klenke, T. Gottschall, R. Klas, C. Rothhardt, S. Demmler, J. Rothhardt, J. Limpert, and A. Tünnermann, "High-average-power femtosecond laser at 258 nm," Opt. Lett. **42**(14), 2826–2829 (2017).
6. H. Xuan, C. Qu, S. Ito, and Y. Kobayashi, "High-power and high-conversion efficiency deep ultraviolet (DUV) laser at 258 nm generation in the $CsLiB_6O_{10}$ (CLBO) crystal with a beam quality of M^2<1.5," Opt. Lett. **42**(16), 3133–3136 (2017).
7. K. Kohno, Y. Orii, H. Sawada, D. Okuyama, K. Shibuya, S. Shimizu, M. Yoshimura, Y. Mori, J. Nishimae, and G. Okada, "High-power DUV picosecond pulse laser with a gain-switched-LD-seeded MOPA and large CLBO crystal," Opt. Lett. **45**(8), 2351–2354 (2020).
8. S. C. Kumar, J. C. Casals, E. S. Bautista, K. Devi, and M. Ebrahim-Zadeh, "Yb-fiber-laser-based, 1.8 W average power, picosecond ultraviolet source at 266 nm," Opt. Lett. **40**(10), 2397–2400 (2015).
9. S. C. Kumar, J. C. Casals, J. Wei, and M. Ebrahim-Zadeh, "High-power, high-repetition-rate performance characteristics of β-BaB_2O_4 for single-pass picosecond ultraviolet generation at 266 nm," Opt. Express **23**(21), 28091–28103 (2015).
10. J. He, D. Lin, L. Xu, M. Beresna, M. N. Zervas, S.-u. Alam, and G. Brambilla, "5.6 kW peak power, nanosecond pulses at 274 nm from a frequency quadrupled Yb-doped fiber MOPA," Opt. Express **26**(6), 6554–6559 (2018).
11. A. Liem, J. Limpert, H. Zellmer, and A. Tünnermann, "100-W single-frequency master-oscillator fiber power amplifier," Opt. Lett. **28**(17), 1537–1539 (2003).

Optics EXPRESS

12. A. V. Harish and J. Nilsson, "Optimization of phase modulation with arbitrary waveform generators for optical spectral control and suppression of stimulated Brillouin scattering," Opt. Express **23**(6), 6988–6999 (2015).
13. G. P. Agrawal, *Nonlinear Fiber Optics*, Academic press (2012).
14. S. Chaitanya Kumar, E. Sanchez Bautista, and M. Ebrahim-Zadeh, "Stable, high-power, Yb-fiber-based, picosecond ultraviolet generation at 355 nm using BiB_3O_6," Opt. Lett. **40**(3), 403–406 (2015).
15. K. Liu, H. Li, S. Qu, H. Liang, Q. J. Wang, and Y. Zhang, "20 W, 2 mJ, sub-ps, 258 nm all-solid-state deep-ultraviolet laser with up to 3 GW peak power," Opt. Express **28**(12), 18360–18367 (2020).
16. S. Wu, G. A. Blake, S. Sun, and H. Yu, "Two-photon absorption inside beta-BBO crystal during UV nonlinear optical conversion," *Nonlinear Materials, Devices, and Applications* 221–227 (2000).
17. M. Takahashi, A. Osada, A. Dergachev, P. F. Moulton, M. Cadatal-Raduban, T. Shimizu, and N. Sarukura, "Improved fourth harmonic generation in β-BaB_2O_4 by tight elliptical focusing perpendicular to walk-off plane," J. Cryst. Growth **318**(1), 606–609 (2011).
18. H. Inagaki, A. Saito, H. Sugiyama, T. Okabayashi, and S. Fujimoto, "Rapid inactivation of SARS-CoV-2 with deep-UV LED irradiation," Emerging Microbes Infect. **9**(1), 1744–1747 (2020).
19. C. Oh, P. P. Sun, E. Araud, and T. H. Nguyen, "Mechanism and efficacy of virus inactivation by a microplasma UV lamp generating monochromatic UV irradiation at 222 nm," Water Res. **186**, 116386 (2020).
20. V. A. R. Huss, H. Festl, and K. H. Schleifer, "Studies on the spectrophotometric determination of DNA hybridization from renaturation rates," Systematic and Applied Microbiology **4**(2), 184–192 (1983).
21. F. Zeng, S. Cao, W. Jin, X. Zhou, W. Ding, R. Tu, S.-F. Han, C. Wang, Q. Jiang, H. Huang, and F. Ding, "Inactivation of chlorine-resistant bacterial spores in drinking water using UV irradiation, UV/Hydrogen peroxide and UV/Peroxymonosulfate: Efficiency and mechanism," J. Cleaner Prod. **243**, 118666 (2020).
22. S. Rattanakul and K. Oguma, "Inactivation kinetics and efficiencies of UV-LEDs against Pseudomonas aeruginosa, Legionella pneumophila, and surrogate microorganisms," Water Res. **130**, 31–37 (2018).
23. Q. Fu, N. Hanrahan, L. Xu, S. Lane, D. Lin, Y. Jung, S. Mahajan, and D. J. Richardson, "Dataset for high-power, high-efficiency, all-fiberized-laser-pumped, 260-nm, deep-UV laser for bacterial deactivation," University of Southampton repository (2021), https://doi.org/10.5258/SOTON/D1981.